Endothelial-Monocyte Activating Polypeptide II, A Novel Antitumor Cytokine that Suppresses Primary and Metastatic Tumor Growth and Induces Apoptosis in Growing Endothelial Cells

By Margaret A. Schwarz,*‡ Jessica Kandel,* Jerald Brett,*† Jun Li,* Joanne Hayward,§ Roderich E. Schwarz,‖ Olivier Chappey,¶ Jean-Luc Wautier,¶ John Chabot,* Paul Lo Gerfo,* and David Stern*

*From the *Department of Pediatrics, the Department of Physiology, and the Department of Surgery, Columbia University, College of Physicians and Surgeons, New York 10032; the ‡Department of Pediatrics and the Department of Surgery, Childrens Hospital of Los Angeles, University of Southern California, Los Angeles, California 90027; §Genentech, Inc., South San Francisco, California 94080; the ‖Department of Surgery, Memorial Sloan-Kettering Cancer Center, New York 10021; and ¶Unité d'Immunohematologie, Laboratoire de Recherche en Biologie Vasculaire et Cellulaire, Université Paris 7, 75475 Paris, France*

Summary

Neovascularization is essential for growth and spread of primary and metastatic tumors. We have identified a novel cytokine, endothelial-monocyte activating polypeptide (EMAP) II, that potently inhibits tumor growth, and appears to have antiangiogenic activity. Mice implanted with Matrigel showed an intense local angiogenic response, which EMAP II blocked by 76% ($P < 0.001$). Neovascularization of the mouse cornea was similarly prevented by EMAP II ($P < 0.003$). Intraperitoneally administered EMAP II suppressed the growth of primary Lewis lung carcinomas, with a reduction in tumor volume of 65% versus controls ($P < 0.003$). Tumors from human breast carcinoma–derived MDA-MB 468 cells were suppressed by >80% in EMAP II–treated animals ($P < 0.005$). In a lung metastasis model, EMAP II blocked outgrowth of Lewis lung carcinoma macrometastases; total surface metastases were diminished by 65%, and of the 35% metastases present, ≈80% were inhibited with maximum diameter <2 mm ($P < 0.002$ vs. controls). In growing capillary endothelial cultures, EMAP II induced apoptosis in a time- and dose-dependent manner, whereas other cell types were unaffected. These data suggest that EMAP II is a tumor-suppressive mediator with antiangiogenic properties allowing it to target growing endothelium and limit establishment of neovasculature.

Key words: tumor • capillary endothelium • programmed cell death • cell growth inhibitors • blood vessels

Murine methylcholanthrene A–induced (meth A)[1] fibrosarcomas, which exhibit spontaneous vascular insufficiency manifested by a heterogeneous pattern of thrombohemorrhage and central necrosis, as well as a failure to form metastatic lesions (1, 2), provide an ideal starting point for isolation of tumor-derived mediators that perturb the vasculature (3–6). We purified a novel cytokine-like molecule, endothelial-monocyte activating polypeptide (EMAP) II, from meth A–conditioned medium based on its capacity to induce activation of endothelial cells (ECs) and mononuclear phagocytes (5, 6). This single chain polypeptide, devoid of a signal sequence, is initially synthesized as an ≈34-kD intracellular precursor, which is processed to the mature ≈20-kD form and released extracellularly by an as yet unidentified pathway. EMAP II showed no significant homology to other known proteins such as cytokines or growth factors. However, an aspartic acid residue is present in the P-1 position in both murine and human EMAP II, suggesting that a cysteine protease in the IL-1β–converting enzyme family might be responsible for producing mature EMAP II from its pro-form. Our ini-

[1]*Abbreviations used in this paper:* bFGF, basic fibroblast growth factor; BrdU, 5-bromodeoxyuridine; DAP-1, 6-diamidino-2-phenylindoledilactate; EC, endothelial cell; EMAP, endothelial-monocyte activating polypeptide; LLC, Lewis lung carcinoma; meth A, methylcholanthrene A–induced fibrosarcoma; RT, reverse transcription; SMC, smooth muscle cell; TUNEL, terminal deoxynucleotidyl transferase–mediated dUTP-biotin nick end labeling; VEGF, vascular endothelial growth factor.

 J. Exp. Med. © The Rockefeller University Press • 0022-1007/99/08/341/13 $5.00
Volume 190, Number 3, August 2, 1999 341–353
http://www.jem.org

tial characterization of EMAP II suggested that its properties resembled those of proinflammatory mediators. For example, EMAP II induced endothelial release of von Willebrand factor, translocation of P-selectin to the cell surface, and synthesis and expression of E-selectin and procoagulant tissue factor (5, 6); these, and EMAP II–mediated activation of cultured monocytes, resulting in production of cytokines and stimulation of cell migration, suggested phlogogenic properties. However, EMAP II administered in vivo, locally or systemically, gave rise to, at most, mild and transient inflammation (6), suggesting that its effects were quite different from those of TNF or IL-1 (2, 7, 8).

In this study we report that EMAP II has antiangiogenic properties preventing blood vessel ingrowth in two experimental angiogenesis models, and suppressing the growth of primary and metastatic tumors without toxicity in normal organs. Consistent with this hypothesis, EMAP II appears to target growing ECs; exposure of growing cultured capillary endothelium to EMAP II induces apoptosis, which is magnified by concomitant hypoxia. These data suggest that EMAP II is a polypeptide with antiangiogenic properties that targets rapidly growing vascular beds.

Materials and Methods

Cell Culture and In Vitro Assays. Bovine aortic and capillary ECs were isolated from calf aortae and adrenal glands, respectively, grown in culture, and characterized based on the presence of vonWillebrand factor and thrombomodulin, as described previously (9). Human umbilical vein ECs (ECV-304 from American Type Culture Collection) were grown in DMEM containing FBS (10%). Bovine vascular smooth muscle cells (SMCs) were prepared by additional scraping of the aortae after removal of the endothelium, and were characterized based on the presence of SMC actin (10). Lewis lung carcinoma (LLC) cells were obtained from American Type Culture Collection and maintained in high glucose DMEM (GIBCO BRL) containing FBS (10%). MDA-MB 468 cells, derived from an estrogen-independent breast carcinoma (HTB 132), were obtained from American Type Culture Collection. EMAP II–induced apoptosis was studied in subconfluent endothelial cultures (9) using the 5-bromodeoxyuridine (BrdU) incorporation kit from Boehringer Mannheim according to the manufacturer's instructions. In brief, cells were incubated for 12 h with BrdU, plated for 24 h on 96-well plates, then treated with either vehicle (FBS, 10%) alone or vehicle plus recombinant (r)EMAP II, as indicated. After 12 or 24 h at 37°C, cells were lysed, centrifuged (250 *g*) for 10 min, and the top 0.1 ml was aspirated and applied to an ELISA plate with preadsorbed anti-DNA antibody. Sites of primary antibody binding were identified using peroxidase-conjugated anti-BrdU antibody. A positive control used purified human recombinant TNF-α (TNF at 10 ng/ml; provided by Knoll Pharmaceuticals). Where indicated, ECs were incubated with rEMAP II and/or exposed to hypoxia ($pO_2 \approx 14$ Torr) using a specially constructed controlled environment chamber, as described previously (11). In addition, the cleavage of the proform of caspase-3 to the active 17-kD form was evaluated in ECs exposed to rEMAP II to assess apoptosis. In brief, subconfluent ECs were incubated with either vehicle or rEMAP II (1 μg/ml) for 24 h at 37°C, and cells were lysed in the presence of protease inhibitors. Equal amounts of protein were then subjected to electrophoresis on a 12% SDS-PAGE gel, transferred to Immobilon-P, blocked overnight in a casein-based blocking solution (Boehringer Mannheim), and probed with a polyclonal rabbit anti–caspase-3 antibody (PharMingen). Specific binding was detected using a chemiluminescence substrate (Pierce Chemical Co.) and XAR-5 film (Eastman Kodak Co.).

Preparation of Recombinant Murine EMAP II, and Detection of EMAP II Transcripts and Antigen. rEMAP II was prepared from *Escherichia coli* (host HMS174[DE3]) transformed with a plasmid containing the coding sequence for mature EMAP II, as described previously (6). Frozen (−80°C) *E. coli* cell paste was mixed 1:10 (wt/vol) with Tris-HCl (20 mM; pH 7.4) containing octyl-β-glucoside (0.1%), and a homogeneous suspension was formed by agitation using a microfluidizer for 20 min (speed 60) at 4°C. Polyethylenimine at pH 7 was then added to the homogenate to a concentration of 0.25%, solids were removed by centrifugation (5,000 *g*; 30 min), and the supernatant was retained. After filtration (0.2 μm), the sample was applied (3 ml sample/ml of gel) to heparin Sepharose CL-4B (Amersham Pharmacia Biotech; 120 ml bed volume) equilibrated in Tris-HCl (20 mM; pH 7.4) containing octyl-β-glucoside (0.1%), and the column was eluted with a linear ascending NaCl gradient. Fractions were pooled on the basis of purity by silver-stained SDS-PAGE, by immunoblotting with antibodies prepared to the NH_2 terminus of mature EMAP II, and by biological activity measured in a tissue factor induction assay (6). The heparin Sepharose pool was concentrated using an Amicon Stirred Cell, and the retentate was desalted into 3-(morpholino)-propane-sulfonic acid (Mops, 25 mM; pH 6.9) and then applied to an SP Sepharose High Performance cation exchange column (55 ml bed volume; Amersham Pharmacia Biotech). The column was eluted by application of a 0–0.5 M ascending linear salt gradient in Mops, and EMAP II–containing fractions were adjusted to 2 M in $(NH_4)_2SO_4$, then applied to a phenyl-Toyopearl 650 M (Tosohaas) column (90 ml bed volume), equilibrated in sodium phosphate (20 mM; pH 7) containing 1 M $(NH_4)_2SO_4$. The column was eluted with a descending salt gradient (2–0 M) in sodium phosphate (20 mM), and EMAP II in the phenyl-Toyopearl column eluate was concentrated to 3–5 mg/ml and formulated into PBS (pH 7.4) by buffer exchange on a Sephadex G25 column (as above). LPS was removed using filtration through a Posidyne filter (Pall Corp.), and LPS levels were estimated using the Endospecy chromogenic assay (limit of detection <10 pg/ml). Purified EMAP II was subjected to NH_2-terminal sequence analysis, mass spectrometry, and SDS-PAGE; the current material was found to be homogeneous according to these criteria. The phenyl-Toyopearl column and Posidyne filtration steps appeared to remove certain toxic contaminant(s) associated with rEMAP II prepared by preparative electrophoresis in previous studies (6). Purified rEMAP II preparations (at a concentration of 1 mg/ml or more) were immediately aliquoted and frozen at −80°C in the presence of mouse serum albumin at a concentration of 1 mg/ml (Sigma Chemical Co.). When an aliquot of rEMAP II was thawed, it was used immediately for experiments (it was not refrozen and used in future studies). These procedures were essential to maintain the bioactivity of rEMAP II.

Antibody to rEMAP II was prepared by standard methods in rabbits (12) and was found to be monospecific, based on immunoblotting of plasma and cell extracts, and that anti-EMAP II IgG blocked the activity of rEMAP II in cell culture assays (6). This antibody was used to develop an ELISA to detect EMAP II antigen by the general protocol described previously (6).

Reverse transcription (RT)-PCR analysis for EMAP II transcripts employed RNA extracted from murine tissues (BALB/c

mice) using the RNA Stat-60 kit (Tel-test, Inc.) according to the manufacturer's instructions, and reverse transcribed (1 μg) using Taq polymerase (Perkin-Elmer Cetus). Primers were used for EMAP II (primer 1, GCATCGCGTCTGGATCTTCGAATT; and primer 2, GTATGTGGCCACACACTCAGCATT) and β-actin (GIBCO BRL). Thermocycling parameters for the experiment shown in Fig. 2 A were as follows: 94°C for 30 s; 55°C for 30 s; and 72°C for 30 s, for a total of 35 cycles. Samples were subjected to agarose gel (1%) electrophoresis, and bands were visualized by ethidium bromide staining. Identity of amplicons was confirmed by Southern blotting with the appropriate cDNA probes. Two negative controls used in PCR experiments included a minus RT control, and a control in which the only DNA present was that from an irrelevant plasmid, the receptor for advanced glycation endproducts (13).

Matrigel and Corneal Neovascularization Models. Matrigel (14, 15; Collaborative Research) containing either vehicle (1% BSA); rEMAP II (100 ng/ml) plus vehicle; basic fibroblast growth factor (bFGF, 100 ng/ml; Collaborative Research) plus heparin (40 U/ml; Sigma Chemical Co.) plus vehicle; rEMAP II (100 ng/ml) plus bFGF/heparin plus vehicle; or heat-inactivated rEMAP II (100 ng/ml; alone or with bFGF/heparin) plus vehicle was mixed at 4°C. Matrigel mixtures were injected subcutaneously into C57BL6/J mice (0.25 ml/site) at two sites per animal. In other experiments, rEMAP II was not added to the Matrigel, but was administered intraperitoneally, either active EMAP II (1 μg every 12 h), heat-inactivated EMAP II (1 μg every 12 h), or vehicle alone, for a total of 14 d. The angiogenic response was analyzed at 14 d after inoculation by routine histology and hemoglobin assay (Sigma Chemical Co.). The number of vessels in 10 high power fields was determined per implant and is expressed as the mean ± SE in each experimental group.

The murine corneal neovascularization model followed the general protocol of Kenyon et al. (16). Pellets for insertion into the cornea were made by combining bFGF (20 mg; Intergen), sucralfate (10 mg; Bukh Meditec), and Hydron polymer in ethanol (0.01 ml of a 12% solution; Interferon Sciences), and applying the mixture to a 15 × 15 mm piece of synthetic mesh (Tetko). The mixture was allowed to air dry, and fibers of the mesh were pulled apart, yielding pellets containing 80–100 ng of bFGF. Pellets containing bFGF were inserted into corneal pockets created 1 mm from the limbus at the lateral canthus of the eye. Mice were then treated with vehicle or EMAP II (1 μg every 12 h) for the next 5 d. After this period, eyes were evaluated for corneal neovascularization; the number of vessels originating in the limbus was counted over the entire orbit, and the area of neovascular response was calculated according to the formula for an ellipse, where $A = [(\text{clock hours}) \times 0.4 \times (\text{vessel length in mm}) \times \pi]/2$. Each clock hour is equal to 30° at the circumference.

Murine Clearance Studies. Clearance of EMAP II in mice was assessed using ^{125}I-labeled rEMAP II. rEMAP II was radioiodinated by the Bolton and Hunter method (3.2 mol of ester/mol of protein [17]), and the tracer was >99% precipitable in TCA (20%), migrated as a single ≈20-kD band on SDS-PAGE, and had a specific radioactivity of ≈8,000 cpm/ng. BALB/c mice received ^{125}I-rEMAP II (0.26 μg) either intravenously via the tail vein or intraperitoneally. Plasma samples were taken, and animals were killed at 24 h. Plasma ^{125}I-rEMAP II concentration data were fit to a two-compartment open model using nonlinear regression by extended least squares analysis (Siphar; SIMED). To assess the "goodness of fit," residual analysis (an examination of the SD) was performed (18).

Murine Tumor Models. For producing primary tumors to test the effects of EMAP II treatment, LLC cells were rinsed with HBSS, trypsinized, counted, resuspended in PBS, and injected subcutaneously into backs of C57BL6/J mice (2×10^6 cells/animal). On the third day after administration of tumor cells, the tumor was reproducibly measurable, and this tumor volume was taken for comparison with later measurements of the same tumor. Animals then underwent intraperitoneal injection every 12 h for 12 d of either vehicle alone (serum albumin, 1%), vehicle plus rEMAP II (at 100 or 1,000 ng), or vehicle plus heat-inactivated rEMAP II (1,000 ng). Tumor growth was assessed with calipers every third day (from days 3–15), and tumor volume was calculated according to the formula for a spherical segment (19), $V = \pi h(h^2 + 3a^2)/6$, where h = height of the segment, a = (length + width)/2, and V = volume (each tumor was compared with itself over multiple measurements, and change in volume was noted). Tumor volume data were analyzed using the Kruskal-Wallis one-way analysis of variance (ANOVA) and a Mann-Whitney mean rank test. Data are expressed as a dimensionless ratio of observed tumor volume divided by initial (day 3) tumor volume. Animals were killed and tumors analyzed histologically at day 15. For primary tumors derived from an estrogen-independent breast carcinoma, MDA-MB 468 cells (2×10^6/animal) were injected subcutaneously into nude mice (NCR Nude from Taconic Farms). On the third day after injection of tumor cells, the tumor was measured, and this tumor volume was used for comparison with later measurements of that tumor as above. Animals underwent intraperitoneal injection every 12 h for 69 d of either vehicle alone (as above), vehicle plus rEMAP II (at 100, 1,000, or 10,000 ng), or vehicle plus heat-inactivated rEMAP II (10,000 ng). Tumor growth was determined every sixth day, and tumor volume was analyzed as above.

For the metastatic tumor model (20, 21), C57BL6/J mice received LLC cells subcutaneously and were observed until tumor volume reached ≥1.5 cm^3. Animals then received rEMAP II (1,000 ng/dose) in vehicle or vehicle alone intraperitoneally every 12 h for 72 h before resection of the primary tumor. After complete resection of the tumor (with no recurrence), mice were observed for an additional 15 d, during which time they received rEMAP II (1,000 ng i.p. every 12 h) in vehicle or vehicle alone (same schedule). On day 15, lungs were injected intratracheally with India ink (15%) to visualize lung surface nodules, and tissue was fixed in Fekete's solution (70% alcohol, 5% glacial acetic acid, 3.7% formaldehyde). Surface metastatic lesions were counted by gross inspection of the tissue under 4× magnification, and macrometastases were defined based on a smallest surface nodule diameter >2 mm.

Tissue Analysis: Histology, Apoptosis, and Immunohistology. Histologic analysis was performed on formalin-fixed, paraffin-embedded tissue, using hematoxylin and eosin staining. The terminal deoxynucleotidyl transferase–mediated dUTP-biotin nick end labeling (TUNEL) assay was used to evaluate apoptosis using the In Situ Cell Death Detection kit (alkaline phosphatase detection system from Boehringer Mannheim). Paraffin-embedded tissue was deparaffinized, rehydrated, and incubated with proteinase K (1 μg/ml) for 30 min. After rinsing with PBS, slides were incubated with TUNEL reaction mixture for 10 min, after which they were exposed to Converter-AP. Alkaline phosphatase was revealed by incubation with substrate (nitroblue tetrazolium [NBT]). For immunolocalization of EMAP II and CD31 antigens, we used rabbit anti-rEMAP II IgG (5 μg/ml) and rat anti–murine CD31 antibody (4 μg/ml; PharMingen). Note that for staining of Matrigel implants for CD31, rabbit polyclonal anti-CD31 IgG (1 μg/ml; provided by Dr. Beat A. Imhof, Basel Institute of Immunology,

Basel, Switzerland) was used. Tissues, fixed as above, were deparaffinized, and underwent peroxide quenching. Using a histostain kit from Zymed Laboratories, after blocking, sections were exposed to anti-CD31 or anti–EMAP II IgG overnight at 4°C. Sections were then incubated with secondary biotinylated antibody as per the manufacturer's protocol. A brief incubation with the Streptavidin-HRP conjugate system (Zymed Laboratories) was followed by development using the chromagen substrate aminoethylcarbazole. Sections were then counterstained with hematoxylin and mounted as indicated.

Results

Distribution of EMAP II in Normal Mice. EMAP II transcripts were demonstrated in a range of organs (brain, liver, lung, spleen, heart, kidney, and smooth muscle; Fig. 1 A), though their levels appeared to be low, requiring PCR amplification to visualize the appropriate size amplicon. Negative controls for PCR amplification of EMAP II transcripts, in which reverse transcriptase was omitted or tissue RNA was replaced with an irrelevant cDNA, demonstrated no band (Fig. 1 A, two far right lanes). Expression of EMAP II transcripts was unaffected by infusion of LPS (100 μg/animal) or induction of hind limb ischemia (data not shown). ELISA for EMAP II antigen showed virtually undetectable levels in the above normal tissues (limit of detection <250 pg/ml) and no peak of EMAP II in the plasma after LPS administration or hind limb ischemia. These data indicated that EMAP II is expressed only at the lowest levels in normal mice, and that it is unlikely to be an early mediator of the host response to acute stimuli such as LPS or ischemia. This clearly contrasts with the rapid production and significant roles for proinflammatory cytokines such as IL-1 and TNF in the acute response to tissue injury (2, 7, 8).

Preparative Scale Purification of rEMAP II. To further study the effects of EMAP II in vitro and in vivo, it was important to develop a preparative scale purification procedure. Previously, we used material eluted from SDS-PAGE corresponding to ≈20,000 M_r. Although this material was highly purified, it was difficult to scale-up such a method, and the biologic properties of the resulting EMAP II were somewhat variable, probably due to differing degrees of denaturation/renaturation during SDS-PAGE and gel elution. This led us to develop an alternate purification strategy. rEMAP II was expressed in *E. coli* (Fig. 1 B, lane 1), and purified by polyethylenimine precipitation, followed by sequential application to heparin Sepharose, SP Sepharose, and phenyl-Toyopearl. Posidyne filtration was then performed to remove LPS (levels were <10 pg at rEMAP II concentrations of 3–5 mg/ml). Details of chromatographic steps are described in Materials and Methods. The final formulated material was homogeneous on SDS-PAGE, migrating as a diffuse band at ≈20 kD (Fig. 1 B, lane 2). Mass spectrometry gave a measured mass of 18,006, which is close to the expected mass of 17,970 (data not shown). NH_2-terminal sequence analysis showed a single sequence with a 100% match between purified murine EMAP II and the published sequence (5, 6).

Effect of EMAP II on bFGF-induced Angiogenesis. To evaluate the ability of EMAP II to regulate blood vessel formation in response to known growth factors, bFGF and heparin were mixed with a gel of basement membrane proteins produced by Engelbreth-Holm-Swarm tumor cells (Matrigel) to serve as a model angiogenic stimulus (14, 15). Subcutaneous Matrigel implants in C57BL6/J mice were evaluated 14 d after inoculation for vessel formation, cellular infiltration, and hemoglobin content. Histologic analysis of the gel showed formation of vessels to be most pronounced and comparable in implants from animals treated with either bFGF/heparin plus vehicle (albumin; data not shown) or bFGF/heparin plus heat-inactivated rEMAP II plus vehicle (Fig. 2 A); higher magnification confirmed the presence of neovessels in these implants (Fig. 2 C). This induction of blood vessel formation is similar to that reported previously with bFGF in this model (15). In contrast, in implants from animals treated with bFGF/heparin plus active rEMAP II, there was marked reduction of vessel ingrowth (Fig. 2, B

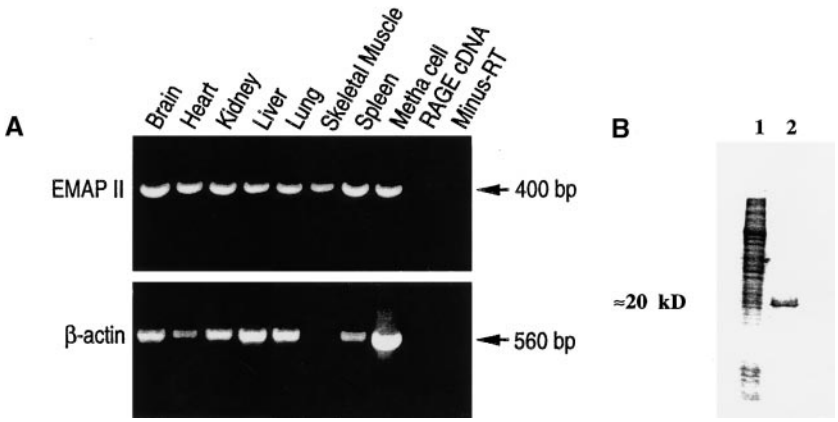

Figure 1. PCR analysis of EMAP II transcripts in normal murine tissue (A) and SDS-PAGE of purified rEMAP II (B). (A) RNA was harvested from normal murine tissues as indicated, and processed for PCR as described in the text. The bands corresponding to the amplicons for EMAP II (400 bp) and β-actin (560 bp) are indicated by arrows. A 100-bp ladder was used as the standard in the far left lane. Negative controls include a lane in which reverse transcriptase was omitted (Minus-RT) and another lane in which irrelevant plasmid DNA (RAGE; reference 13) was added in place of sample DNA (two far right lanes). (B) *E. coli* homogenate and purified rEMAP II were subjected to reduced SDS-PAGE (10–20% Tricine gels; 10 μg/lane), and protein was visualized by Coomassie blue. Lane 1, *E. coli* homogenate after centrifugation (12,000 *g*); lane 2, rEMAP II formulated into PBS. Migration of simultaneously run molecular weight standards is indicated in kD.

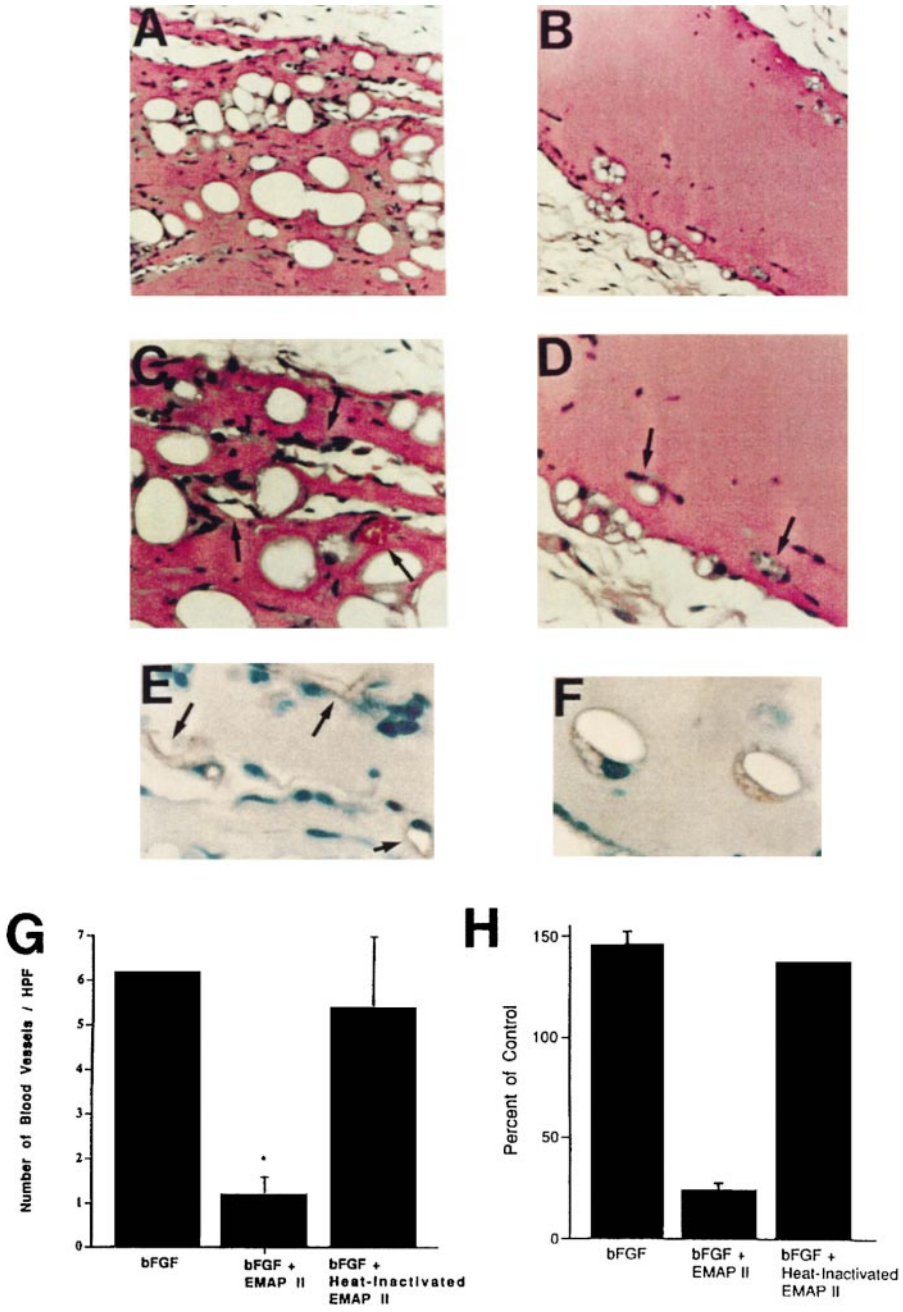

Figure 2. Matrigel angiogenesis model: effect of rEMAP II on bFGF-induced neovascularization. Mice received subcutaneous Matrigel implants and were killed after 14 d to analyze new vessel formation by histologic examination and hemoglobin assay. (A, C, and E [arrows in C indicate vessels denoted in E]) Implant containing bFGF/heparin plus heat-inactivated rEMAP II (100 ng/ml) plus vehicle. (B, D, and F [arrows in D indicate vessels seen in F]) Implant containing bFGF/heparin plus rEMAP II (100 ng/ml) plus vehicle. (G) The density of vessels in Matrigel implants, under the conditions described above (A–F), was determined by counting 10 high power fields (HPF) of sections stained with anti-CD31 antibody (mean ± SE is shown). (H) Results of hemoglobin assay (reported as percentage of control; Matrigel with vehicle arbitrarily defined as 100%). Note that the bar designated bFGF refers to implants containing bFGF/heparin alone. Results were evaluated by Student's *t* test; $P < 0.001$ comparing hemoglobin levels in the presence of rEMAP II with control and bFGF groups. There is a statistically significant decrease in vessel counts in Matrigel implants containing EMAP II compared with control or those containing heat-inactivated EMAP II (*$P < 0.0001$ by Kruskal-Wallis). These experiments were repeated seven times. Original magnifications: A and B, 87.5×; C and D, 200×; E and F, 400×.

and D), i.e., little to no vessel formation ($n = 40$; this experiment was performed seven times). Vessel confirmation was established by use of CD31 (Fig. 2 E, vehicle plus heat-inactivated EMAP II plus bFGF; and Fig. 2 F, vehicle plus EMAP II plus bFGF). Consistent with these histologic findings, there was a 76% reduction in hemoglobin content in corresponding implants containing bFGF/heparin plus rEMAP II, compared with bFGF/heparin plus vehicle or heat-inactivated EMAP II plus bFGF/heparin plus vehicle (Fig. 2 H). Matrigel implants were scored for the mean number of vessels per 10 high power fields. When rEMAP II was present, vessel density was reduced ($P < 0.0001$ by Kruskal-Wallis; Fig. 2 G), consistent with the results of the hemoglobin assay. Further experiments were also done to be certain that the observed effects in the Matrigel model were not due to potentially toxic high local concentrations of rEMAP II in the implant itself. For these studies, animals received Matrigel implants containing bFGF/heparin, followed by intraperitoneally administered rEMAP II (1 μg every 12 h for 14 d), heat-inactivated rEMAP II (same dose), or vehicle alone. Results were analogous to those described above; treatment with rEMAP II suppressed vascular ingrowth into the Matrigel, whereas heat-inactivated EMAP II or vehicle alone had no effect (data not shown).

In view of our previous in vitro studies with EMAP II (5, 6), in which it initially appeared to have properties of an inflammatory mediator, the results of these experiments in the Matrigel model were unexpected. This led us to

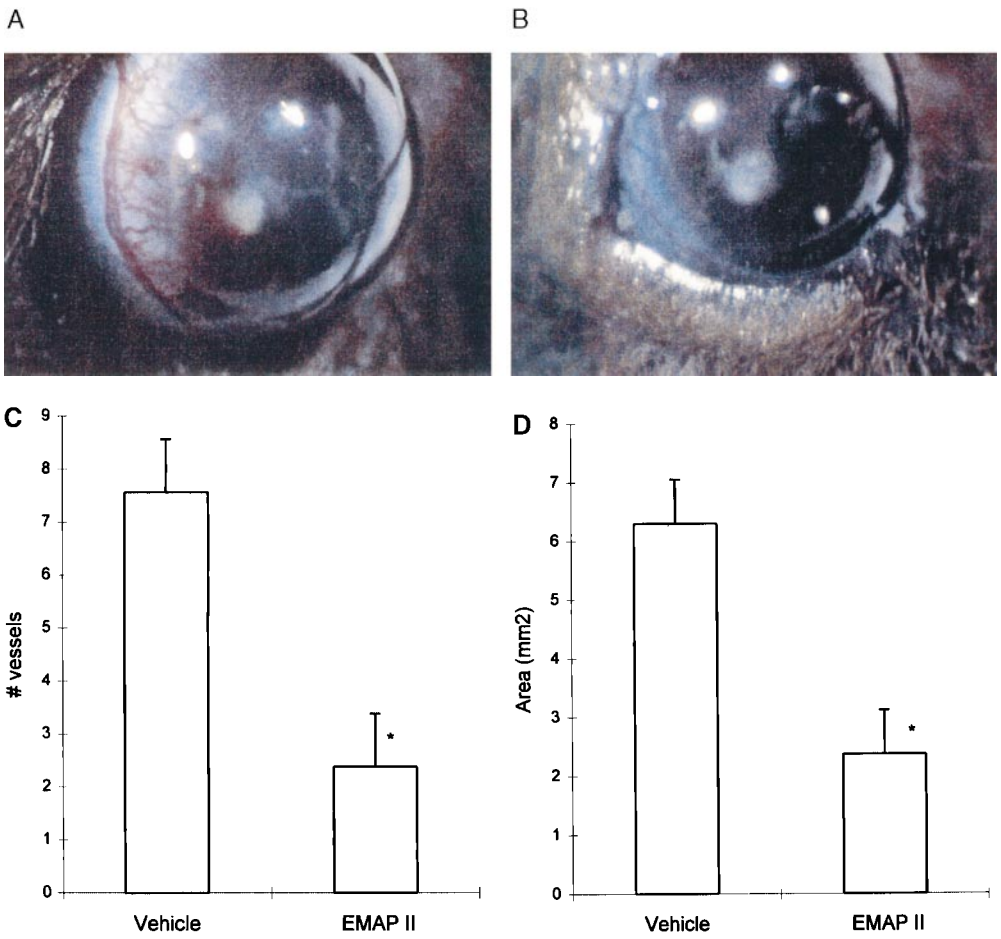

Figure 3. Corneal neoangiogenesis model: effect of rEMAP II on bFGF-induced neovascularization. Hydron pellets containing bFGF (≈90 ng) were implanted in corneal pockets. Mice were then treated with EMAP II (2 μg i.p. every 24 h for 5 d; B) or vehicle (A), and the corneal neovascular response was assessed. The total number of neovessels originating in the limbus was counted (C; $*P < 0.003$), and the area of neovascularization was calculated (D; $*P < 0.002$). Data shown are the results of 16 observations in 8 animals in each of the experimental groups, for a total of 32 observations in 16 animals. The experiment was repeated twice.

confirm these observations in another neovascularization model, namely that using the mouse cornea (16). For these studies, bFGF was incorporated into slow-release polymer pellets (Hydron) which were implanted into corneal pockets of mice. Animals then received rEMAP II (2 μg/d every 24 h) or vehicle alone intraperitoneally for 5 d. Corneal neovascularization was evident in animals receiving vehicle (Fig. 3 A), and was markedly suppressed by treatment with rEMAP II (Fig. 3 B). This initial impression was confirmed by counting the number of neovessels originating in the limbus (Fig. 3 C) and by determining the area of corneal neovascularization (Fig. 3 D); in each case, ≈60% suppression of vessel ingrowth was observed. Taken together, these data in the Matrigel implant and corneal neovascularization models suggested that rEMAP II had the capacity to suppress neovessel formation in response to bFGF.

Plasma Clearance and Tissue Deposition of Infused rEMAP II. To perform further in vivo studies with rEMAP II, its plasma clearance was evaluated. Clearance studies were performed using either intravenously or intraperitoneally administered ^{125}I-rEMAP II (Fig. 4). The fall in plasma concentration of ^{125}I-rEMAP II after intravenous injection best fit a biexponential function (18); the distribution and elimination half-lives were 0.47 ± 0.17 and 103 ± 5 min, respectively. After intraperitoneal injection, ^{125}I-EMAP II was detected in plasma after 1 min, and the maximum concentration was reached by 35 ± 10 min. The resorption phase of rEMAP II handling in vivo was best described as a first-order process. The elimination phase after intraperitoneal administration fit to a monoexponential decline, and the resorption and elimination half-lives were 50.1 ± 0.1 and 102 ± 6 min, respectively.

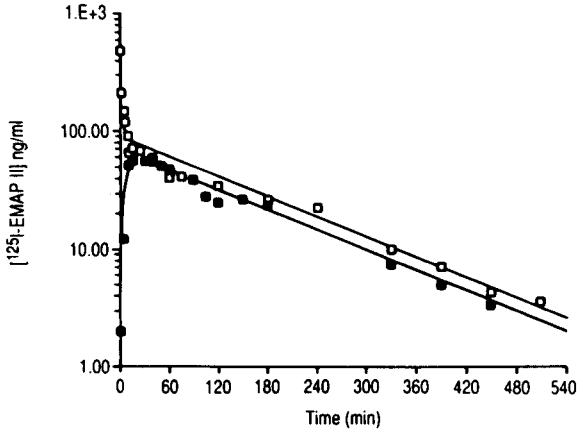

Figure 4. Disappearance of ^{125}I-EMAP II from mouse plasma after intravenous (□) or intraperitoneal (■) infusion. Mice received ^{125}I-EMAP II (0.26 μg/ml) by either intravenous or intraperitoneal injection, and plasma was sampled at the indicated time points. The method for data fitting and parameters of clearance are described in the text.

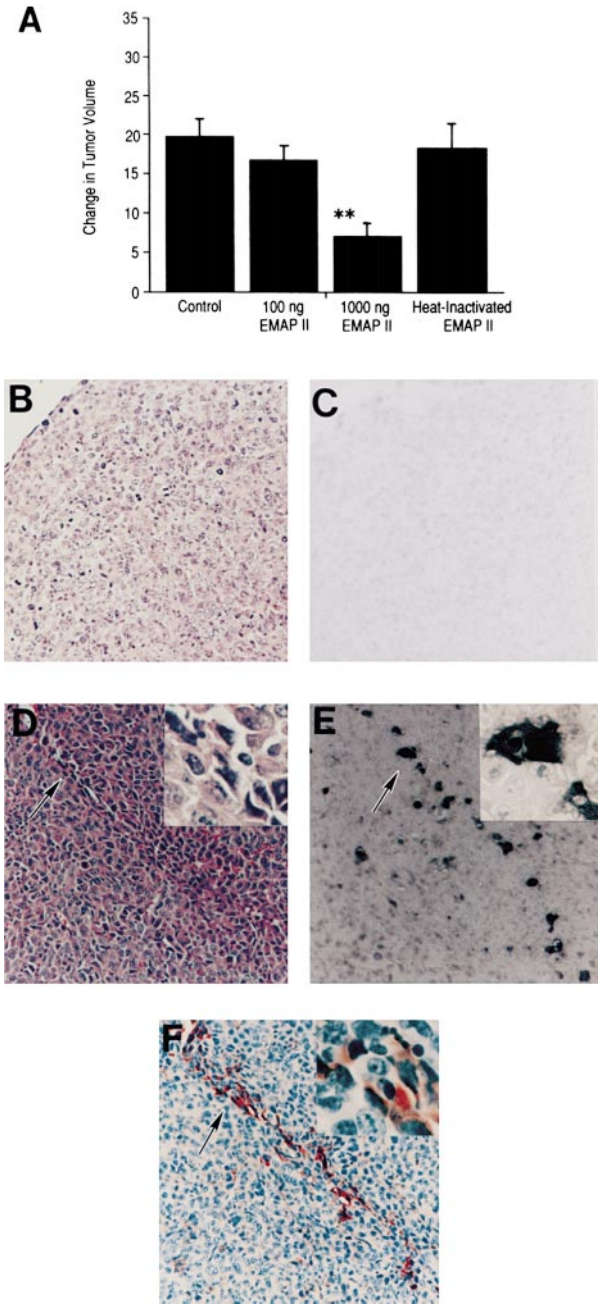

Figure 5. Effect of rEMAP II on primary LLCs. Mice were injected subcutaneously on day 1 with LLC cells, and then on days 3–15 were treated intraperitoneally every 12 h with either vehicle alone (control), rEMAP II (100 or 1,000 ng), or heat-inactivated rEMAP II (1,000 ng). (A) Change in tumor volume in each of the four groups (mean ± SE) is shown ($n = 40$), and data analysis was performed as described in the text (**: $P < 0.034$, Kruskal-Wallis; and $P < 0.003$, Mann-Whitney). The volume of tumor (in mm^3) on day 3 was as follows: control group, 10.2 ± 2.3 (mean ± SD); rEMAP II–treated (100 ng) group, 9.8 ± 2.6; rEMAP II–treated (1,000 ng) group, 10.3 ± 2.2; heat-inactivated rEMAP II group, 9.2 ± 2.8. Data are expressed as a dimensionless ratio of tumor volume on day 15 to that on day 3 (each animal compared only with itself). (B–F) Representative sections of LLC tumors harvested from mice treated with vehicle alone (B and C) or rEMAP II (1,000 ng; D–F) on day 15. In F (arrow indicates the area of inset at higher magnification), the association of pyknotic areas observed in D (arrow indicates the area of inset at higher magnification) with sites of microvessels was confirmed by staining sequential sections with anti-CD31 IgG. In E (arrow indicates the area of inset at higher magnification), TUNEL staining of adjacent sections demonstrates apoptotic nuclei in the region with multiple microvessels. These results in rEMAP II–treated tumors contrast with the uniform appearance of untreated tumors (B and C) and their lack of apoptotic areas after TUNEL staining of sections (C). These experiments were repeated three times. Original magnifications: B–F, 87.5×; D–F insets, 400×.

Effect of rEMAP II on Growth of Primary and Metastatic Tumors. Mice implanted subcutaneously with LLC cells developed tumors which were first measured when they achieved a volume of ~9–10 mm^3, ≈3 d after inoculation of cells. The volume of each tumor was then measured every third day and compared with the initial volume of that tumor on day 3. Compared with tumor-bearing animals treated with vehicle alone or vehicle plus heat-inactivated EMAP II, mice receiving active rEMAP II showed a striking reduction in tumor volume (Fig. 5 A). Differences between tumor volume in control and EMAP II–treated animals were statistically significant using either the Kruskal-Wallis one-way ANOVA ($P < 0.034$) or comparing control versus high dose rEMAP II by Mann-Whitney analysis ($P < 0.003$). Histologic study of LLC tumors allowed to grow for 15 d and injected intraperitoneally every 12 h with vehicle (albumin, 1%) demonstrated a densely packed and uniform cell population (Fig. 5 B). Tumors from animals receiving heat-inactivated rEMAP II (at 1,000 ng/dose) were similar in appearance to vehicle controls (data not shown). After administration of rEMAP II at 1,000 ng/dose twice daily for 12 d, areas of pyknosis were observed in the tumor bed (Fig. 5 D). At higher magnification, rEMAP II–induced areas of pyknosis had a general perivascular distribution (Fig. 5 D, inset). In Fig. 5, D, E, and F, the close association of pyknotic areas in the tumor (D), localization of the vascular marker CD31 (F), and evidence of DNA fragmentation using the TUNEL assay (E) are observed (through the use of sequential sections). There were no such apoptotic areas in control tumors treated with vehicle alone (Fig. 5 C). There was a dose-dependent increase in apoptotic areas present in the tumors with 100 and 1,000 ng of EMAP II. Mice treated with rEMAP II were normally active, continued food/water consumption, and maintained their weight comparably to control mice.

To determine whether the tumor-suppressive effect of rEMAP II could be extended to human tumors, the MDA-MB 468 cell line, derived from an estrogen-independent breast carcinoma (HTB 132) was used to establish subcutaneous tumors in nude mice. Mice were treated with either of three doses of rEMAP II (100, 1,000, or 10,000 ng/12 h i.p.), heat-inactivated rEMAP II (10,000 ng/12 h i.p.), or vehicle alone for 69 d after the same protocol as for the LLC tumors (Fig. 6, A and B). A concentration-dependent inhibition of tumor volume was observed in the presence of rEMAP II that was most striking and reached a plateau at the two higher doses (1,000 and 10,000 ng; $P < 0.01$ by Mann-Whitney and $P < 0.001$ by Kruskal-Wallis). There was no evidence of toxicity over the almost 10-wk period of rEMAP II administration.

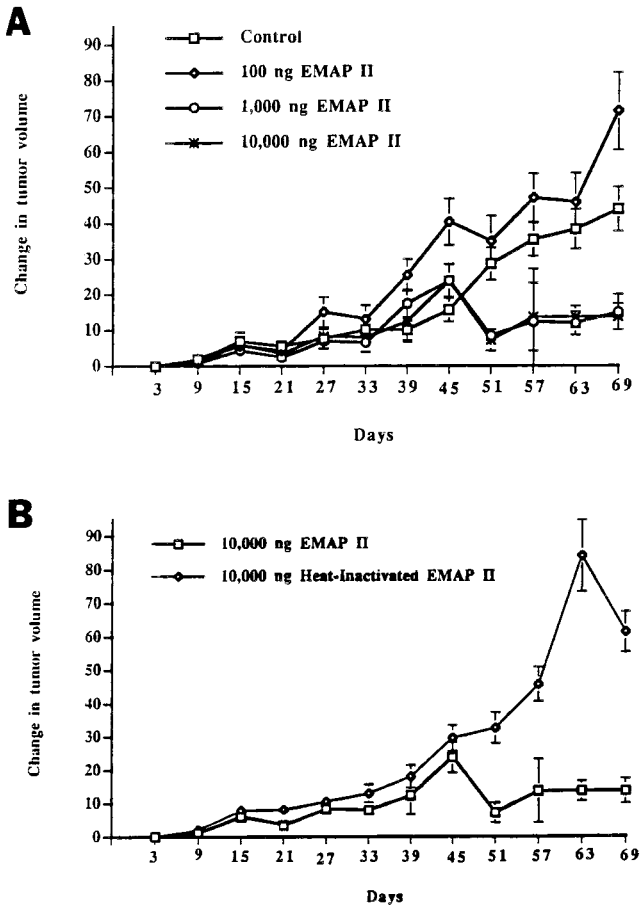

Figure 6. Effect of rEMAP II on tumors derived from MDA-MB 468 cells. Nude mice were injected subcutaneously on day 1 with MDA-MB 468 cells, and then on days 3–69 were treated intraperitoneally every 12 h with either vehicle alone (Control), rEMAP II (100, 1,000, or 10,000 ng), or heat-inactivated rEMAP II (10,000 ng). Change in tumor volume in each of the five groups (mean ± SE) is shown ($n = 50$), and data analysis was performed as described in the text ($P < 0.005$ by Mann-Whitney, and $P < 0.001$ by Kruskal-Wallis compared with controls). The volume of tumor (in mm^3) on day 3 was as follows: control group, 2.9 ± 1.3 (mean ± SD); rEMAP II–treated (100 ng) group, 2.5 ± 1; rEMAP II–treated (1,000 ng) group, 4.4 ± 1.2; rEMAP II–treated (10,000 ng) group, 4.4 ± 1.2 (A); rEMAP II–treated (10,000 ng) group, 3.5 ± 1.3; heat-inactivated rEMAP II group, 2.6 ± 1.1 (B). Data are expressed as a dimensionless ratio of tumor volume on the indicated day compared with day 3 (each animal compared only with itself). These experiments were repeated three times.

As established metastatic foci require blood vessel ingrowth to expand beyond 1–2 mm (22–25), we reasoned that rEMAP II might suppress growth of metastatic lesions. The LLC model was used by allowing primary tumors to grow to a volume of ≥1.5 cm^3, at which time metastases are present (but suppressed by the primary tumor [19, 20]). Then, the primary lesion was resected (with no recurrence at the site of resection), and analysis of surface lung nodules was undertaken 15 d later. rEMAP II treatment was begun 72 h before resection of the primary tumor and continued through the end of the experiment. Animals receiving rEMAP II (1,000 ng i.p. every 12 h; Fig. 7, B and D, arrow indicates area of inset) showed significantly fewer and smaller surface nodules, compared with vehicle (Fig. 7, A and C) by gross inspection and histologic study. Consistent with these data, rEMAP II–treated animals demonstrated 65% suppression ($P < 0.009$ by Mann-Whitney) in outgrowth of the total number of surface metastases, compared with mice receiving vehicle alone (Fig. 7 E). Of the 35% of metastases present in rEMAP II–treated animals, ≈80% of these metastases were inhibited, such that the maximum diameter was <2 mm (i.e., predominately micrometastases were present) compared with controls ($P < 0.002$ by Student's *t* test; Fig. 7 E, inset).

Effect of rEMAP II on Endothelium. Our data thus far demonstrated an association of EMAP II with induction of apoptosis in tumors, the latter at least in part in a perivascular distribution. These data suggested the possibility that tumor vasculature might be a target of EMAP II. ELISA for DNA fragmentation was performed to more precisely delineate apoptotic effects of rEMAP II on growing cultured endothelium. There was a dose-dependent increase in DNA fragmentation in cultured bovine capillary endothelium, reaching 250% over that observed in controls within 24 h (Fig. 8 A). As tumor tissue is also known for the presence of areas of local tissue hypoxia/hypoxemia (26, 27), we assessed whether rEMAP II might display enhanced activity under oxygen deprivation. When cultured subconfluent capillary ECs were exposed to hypoxia ($pO_2 \approx 14$ Torr), DNA fragmentation was accelerated, reaching a level of 250% above that observed with vehicle alone within 12 h (rather than the 24 h required for an effect of this magnitude in normoxia; Fig. 8 A). This was consistent with the accelerated appearance of apoptotic bodies by 6-diamidine-2-phenylindoledilactate (DAP-1) staining of hypoxic cultured capillary endothelial cultures exposed to rEMAP II. Controls in which bovine capillary ECs were treated with heat-inactivated rEMAP II, in place of active rEMAP II, showed no induction of apoptosis (data not shown). Induction of apoptosis after exposure to rEMAP II was not as striking in cultured bovine aortic or human umbilical venous ECs, where a maximum of ≈50% apoptosis over untreated controls was observed at the highest concentrations of rEMAP II tested (Fig. 8 B; analysis by Student's *t* test showed no statistical significance). In contrast, LLC or MDA-MB 468 cells, and nontransformed vascular SMCs demonstrated no increase in DNA fragmentation after exposure to rEMAP II under the conditions above by ELISA (Fig. 8 C) or DAP-1 staining (data not shown). Consistent with the observed induction of apoptosis in ECs, we noted that rEMAP II induced activation of the cytosolic protease caspase-3 to its active 17-kD form found in cells undergoing apoptosis (Fig. 8 D).

Discussion

Neovascularization is a critical regulator of the growth of both primary and metastatic neoplasms (22–25). Earlier studies called attention to the role of angiogenic factors, such as vascular endothelial growth factor (VEGF [28–30]), acidic FGF (31), bFGF (32), and angiogenin (33–35), in promoting tumor

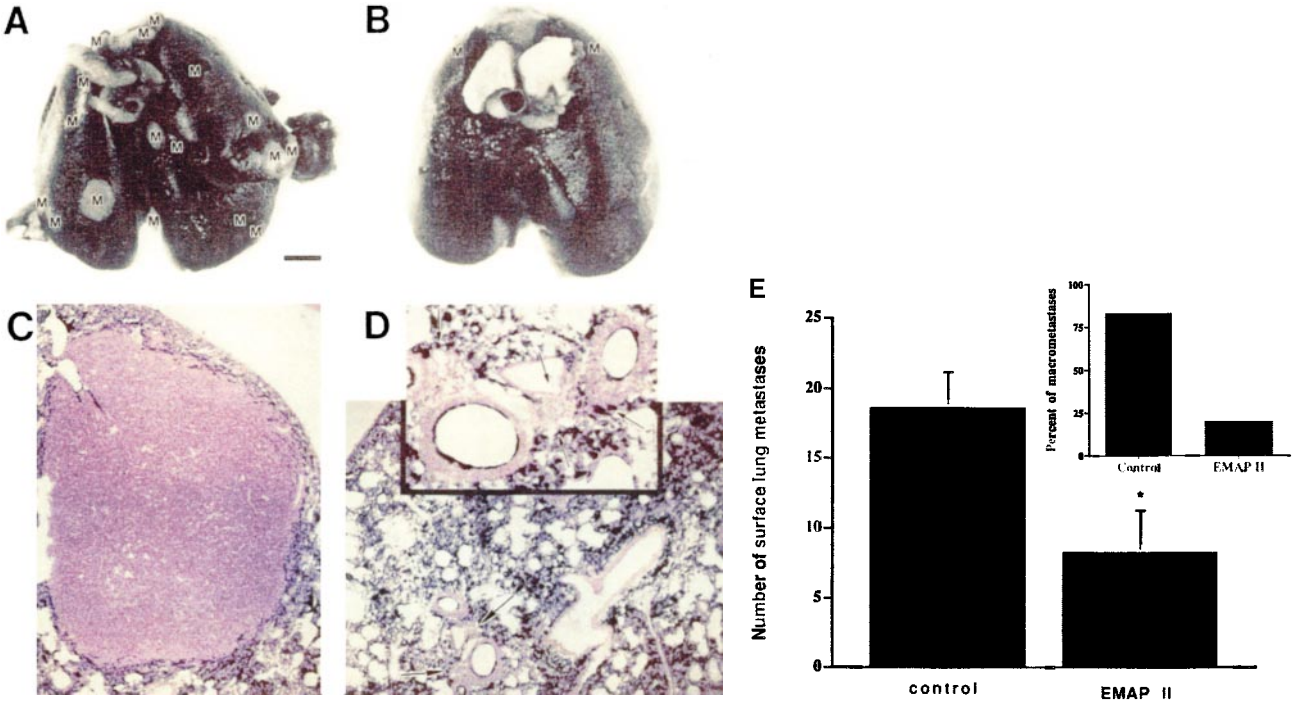

Figure 7. Lung metastasis model with LLC. Mice received LLC cells subcutaneously and were observed until tumors reached a volume of ≥1.5 cm^3, at which time animals were treated with rEMAP II (1,000 ng i.p. every 12 h; $n = 8$) or vehicle alone (control; $n = 6$) for 72 h. Tumors were subsequently resected (there were no local recurrences), and the same treatment regimen was continued for the duration of the study, an additional 15 d. India ink was instilled intratracheally to enhance visualization of metastases (pale areas) compared with normal tissue (dark areas). Gross appearance of lungs demonstrated many surface macrometastases in controls (A) versus their marked suppression in rEMAP II–treated mice (B). Histologic examination confirmed this impression (C, vehicle-treated; D, EMAP II–treated; arrow in D and inset in D indicate the presence of micrometastasis). (E) Surface lung metastasis/nodule data from all animals were analyzed using Mann-Whitney (*$P < 0.009$). Total surface metastases are shown in the main figure (mean ± SE), and surface macrometastases (>2 mm; mean ± SE for control and EMAP II–treated groups were 80 ± 12.5 and 20 ± 13%, respectively), counted using a calibrated ocular, are shown in the inset (by Student's t test, $P < 0.002$). These experiments were repeated four times. Bar (A and B): 1 cm; original magnifications: C and D, 87.5×; D inset, 200×.

growth and establishing metastases. For example, in a transgenic murine model, a switch in phenotype from benign fibroma to malignant fibrosarcoma was closely tied to expression of angiogenic mediators (36), and antibody to VEGF inhibited growth of explanted human tumors in athymic mice (29, 30). Similar inhibition of experimental tumor growth has also been observed with antibodies to angiogenin (35) and bFGF (37). Alternatively, recent work has identified endogenous peptides with antiangiogenic activities, including angiostatin (20), thrombospondin (38), and glioma-derived angiogenesis inhibitory factor (39). They can inhibit tumor growth either at the primary tumor site (thrombospondin [38]) or at a site of distant metastases (angiostatin [20, 40]). Formation of the tumor vascular bed, as well as blood vessel formation in other situations, such as in ischemia, wound healing, and atherosclerosis (41–44), is presumably also controlled by the interaction of such positive and negative stimuli on endothelium in diverse vascular beds.

Carcinogen-induced murine meth A and similar tumors (1, 2) are ideally suited to the analysis of host–tumor interactions because short-term vascular insufficiency (exaggerated by concomitant administration of an agent such as TNF) and longer-term immunologic mechanisms limit local tumor growth (1, 2, 45–48). In fact, acute local (intratumor) administration of EMAP II to meth A tumors resulted in thrombohemorrhage in the tumor bed (6), a finding quite distinct from what we observed in the current study in which EMAP II was administered systemically at lower doses over longer time periods. Consistent with the ability of EMAP II to modulate vessel integrity was the observation that neovessel formation into bFGF-containing implants was blocked by rEMAP II. In contrast to these results with rEMAP II, other cytokines such as TGF-β or TNF-α have been found to induce vascular ingrowth in angiogenesis models (49–51).

In the LLC model, rEMAP II attenuated growth of primary tumors and resulted in a histologic picture of apoptotic tissue injury, at least in part in a perivascular distribution, which progressed to nonviable tumor, probably as a result of severe ischemia. The observation that apoptosis in EMAP II–treated tumors extended beyond the vasculature raises the possibility of a paracrine effect whereby results of EC–EMAP II action might cause release of factors toxic to nearby cells. In support of the suggestion that EMAP II was initially targeting the vasculature, we found that rEMAP II also markedly attenuated growth of a human breast carcinoma line (MDA-MB 468) grown in nude mice. The finding that EMAP II diminished lung surface metastases, and, especially, macrometastases, is also consistent with the concept that neovasculature feeding the tumor, as well as in the tumor, is a target of EMAP II. It is notable that despite a

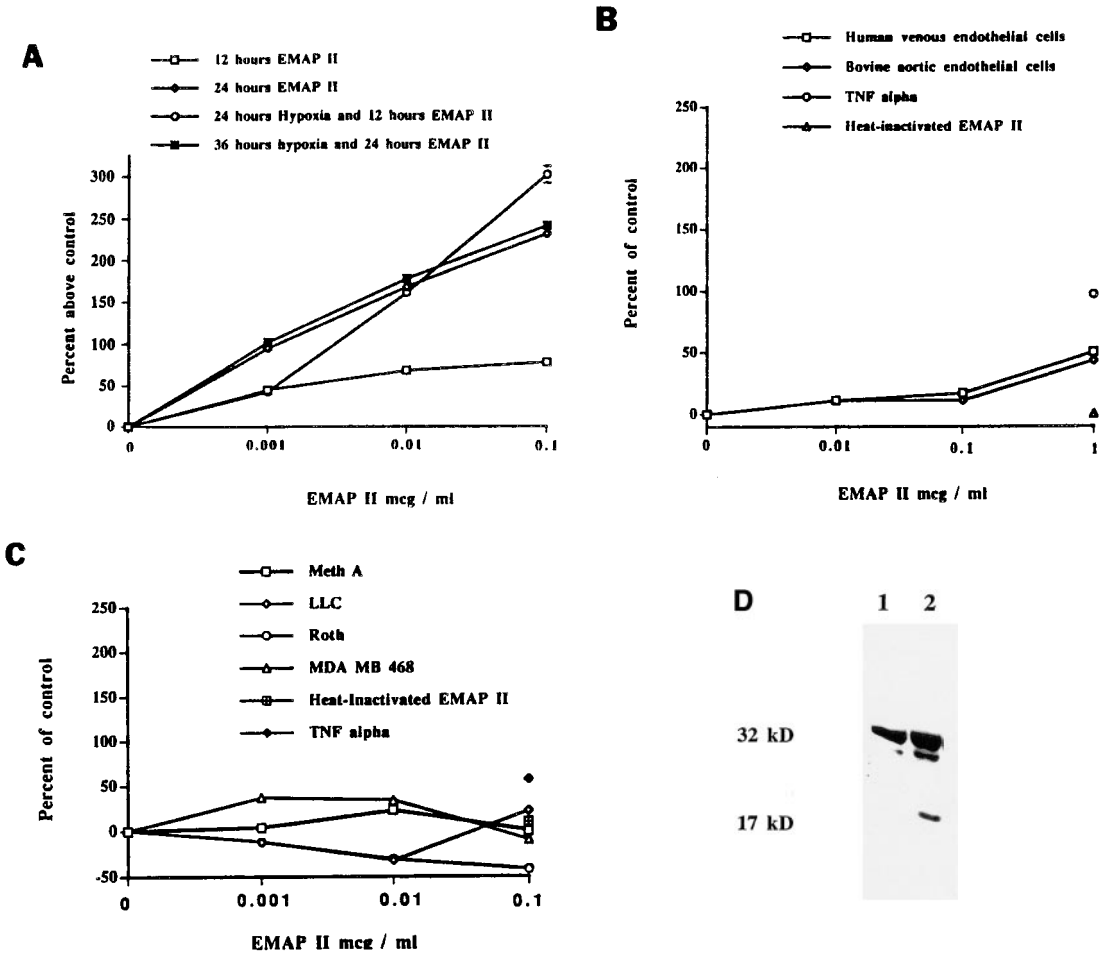

Figure 8. Effect of EMAP II on cultured ECs. (A) DNA fragmentation by ELISA of subconfluent cultured bovine capillary ECs in normoxia or hypoxia ($pO_2 \approx 14$ Torr), exposed to rEMAP II as indicated or heat-inactivated EMAP II (data not shown). (B) The same experiments were performed with subconfluent bovine aortic and venous ECs. (C) The ELISA for DNA fragmentation was performed on LLC, MDA-MB 468, meth A, or vascular SMCs after 24 h of exposure to EMAP II. Data shown represent mean and, in each case, SE was <10%. Experiments with bovine capillary ECs and bovine aortic/venous ECs were repeated three and two times, respectively. (D) ECs exposed to rEMAP II had activation of caspase-3 (lane 2) found in cells undergoing apoptosis compared with control (lane 1).

prolonged course of rEMAP II treatment, ≈10 wk, no untoward effects on general health of the animals was observed, and pathologic analysis of normal organs revealed no lesions. This suggested that actions of EMAP II were localized, under these conditions, to the tumor. However, our data do not rule out the possibility that EMAP II may have other effects on the tumor beyond that on the vasculature. For example, the action of EMAP II on endothelium or other elements in the tumor microenvironment might release diffusible mediators toxic for tumor cells, thus causing tumor injury initially close to the vasculature, but then extending deeper into the tumor.

A salient feature of tumor vasculature, which distinguishes vessels in the tumor stroma from those in normal tissue, is the increased fraction of growing/migrating ECs (22–24). Our studies in cell culture suggested an effect of rEMAP II focused on growing capillary endothelium, predominately induction of apoptosis, supported by our observation that there was activation of caspase-3, a key protease that is triggered during the early stages of apoptosis. In contrast, bovine aortic and venous endothelium was less susceptible to the effects of EMAP II. Furthermore, addition of the cytokine to cultures of growing tumor cells (LLC or MDA-MB 468) showed no change in cell proliferation or induction of apoptosis, though rEMAP II suppressed these tumors in vivo. Enhanced EMAP II–induced apoptosis in hypoxic endothelial cultures provided further support for the relevance of our finding to tumor biology, as the presence of hypoxic areas in tumors is well established (26, 27). On a cellular level, hypoxia could potentially sensitize endothelium to EMAP II by several mechanisms, including arrest of cells at the G1/S interface (11) or increased sensitivity to subsequent encounters with oxidizing stimuli. In support of the latter hypothesis, pilot studies suggest that EMAP II has an important effect on cellular redox status, as addition of *N*-acetylcysteine blocks EMAP II–mediated endothelial apoptosis. Analysis of mechanisms through which EMAP II induces possible cellular oxidant stress, further definition of the caspase pathway, and

elucidation of the cell surface receptor for EMAP II will provide more definitive answers to questions concerning the specificity and selectivity of its cellular effects.

The striking feature of our in vivo studies is the suppressive effect of rEMAP II on tumors without, apparently, an adverse affect on the function of normal organs. We suggest that this is due to EMAP II's effect on the endothelium; EMAP II could perturb endothelium in vivo not only by direct effects on endothelial apoptosis, but also by other means. For example, EMAP II–mediated induction of endothelial tissue factor could trigger local activation of clotting in the tumor bed, thereby diminishing blood flow and enlarging the volume of tumor at risk for ischemia. EMAP II might also modulate the expression of other mediators that control the local angiogenic balance, including enhanced activity of pathways regulating production of angiostatic peptides, such as angiostatin or thrombospondin, and/or might suppress expression of proangiogenic factors in the tumor bed. Furthermore, EMAP II might elicit endothelial production of mediators that directly impair tumor cell viability (as mentioned above). Though there are many mechanistic, physiologic, and practical questions to be explored in future studies (e.g., whether EMAP II will affect well-established vessels in human tumors that grow over much longer time periods than the accelerated murine models; or whether an optimal antitumor regimen of EMAP II will induce tumor regression or just be static), our data support the potential of EMAP II, a cytokine with apparent antiangiogenic properties, to suppress primary and metastatic tumor growth, and to induce apoptosis in the tumor without apparent adverse affects on normal organs.

The authors acknowledge the work of Dr. Janet Kao, which was crucial for the initial identification and characterization of EMAP II. We are grateful for Dr. Gabriel Godman's suggestions throughout the course of this work and preparation of the manuscript. Bovine capillary ECs were generously provided by Dr. J. Folkman (Harvard Medical School, Brookline, MA).

This work was supported by grants from the U.S. Public Health Service (HL42833, PERC; to D. Stern), the Naboa Surgical Research Fund, and the National Institutes of Health (HL60061 and HL03981, KO2; to M. Schwarz). M. Schwarz completed this work during the tenure of a Clinician-Scientist Award from the American Heart Association with funds contributed in part by the New York affiliate.

Address correspondence to Margaret Schwarz at her current address, Departments of Pediatrics and Surgery, Children's Hospital Los Angeles, 4650 Sunset Blvd. MS #66, Los Angeles, CA 90027. Phone: 323-669-4148; Fax: 323-913-2865; E-mail: mschwarz@chla.usc.edu

R. Schwarz's current address is Department of General Oncologic Surgery, City of Hope National Medical Center, 1500 East Duarte Rd., Duarte, CA 91010.

Submitted: 2 March 1999 Revised: 24 May 1999 Accepted: 2 June 1999

References

1. Old, L. 1986. Tumor necrosis factor. *Science*. 230:630–632.
2. Old, L., B. Benacerraf, D. Clarke, E. Carswell, and E. Stockert. 1961. Role of the reticuloendothelial system in the host reaction to neoplasia. *Cancer Res*. 21:1281–1300.
3. Clauss, M., C. Murray, M. Vianna, R. deWaal, G. Thurston, P. Nawroth, H. Gerlach, M. Gerlach, R. Bach, P. Familletti, and D. Stern. 1990. A polypeptide factor produced by fibrosarcoma cells that induces endothelial tissue factor and enhances the procoagulant response to TNF. *J. Biol. Chem*. 265:7078–7083.
4. Clauss, M., M. Gerlach, H. Gerlach, J. Brett, F. Wang, Y.-C. Pan, P. Familletti, J. Olander, D. Connolly, and D. Stern. 1990. VPF: a tumor-derived polypeptide which induces endothelial cell and monocyte procoagulant activity and promotes monocyte migration. *J. Exp. Med*. 172:1535–1545.
5. Kao, J., J. Brett, G. Godman, J. Chen, P. Familletti, J. Wang, Y.-C. Pan, D. Stern, and M. Clauss. 1992. Endothelial-monocyte activating polypeptide (EMAP) II. *J. Biol. Chem*. 267:20239–20247.
6. Kao, J., K. Houck, Y.-G. Fan, J. Brett, I. Haehnel, M. Kayton, T. Grickscheit, S. Libutti, J. Chabot, R. Nowgrod, et al. 1994. Characterization of a novel tumor-derived cytokine: EMAP II. *J. Biol. Chem*. 269:25106–25119.
7. Sherry, B., and A. Cerami. 1988. TNF exerts endocrine, paracrine, and autocrine control of inflammatory responses. *J. Cell Biol*. 107:1269–1277.
8. Dinarello, C., and C. Wolff. 1993. The role of interleukin 1 in disease. *N. Engl. J. Med*. 328:106–113.
9. Gerlach, H., H. Lieberman, R. Bach, G. Godman, J. Brett, and D. Stern. 1989. Enhanced responsiveness of endothelium in the growing/motile state to TNF. *J. Exp. Med*. 170: 913–931.
10. Gown, A., A. Vogel, D. Gordon, and P. Lu. 1985. A smooth muscle cell-specific monoclonal antibody recognizes smooth muscle actin isozymes. *J. Cell Biol*. 100:807–813.
11. Shreeniwas, R., S. Ogawa, F. Cozzolino, G. Torcia, N. Braunstein, C. Butura, J. Brett, H. Lieberman, M. Furie, J. Joseph-Silverstein, and D. Stern. 1991. Macrovascular and microvascular endothelium during long-term hypoxia: alterations in cell growth, monolayer permeability, and cell surface coagulant properties. *J. Cell. Physiol*. 146:8–17.
12. Vaitukatis, J. 1981. Production of antisera with small doses of

immunogen: multiple intradermal injections. *Methods Enzymol*. 73:46–52.
13. Neeper, M., A.-M. Schmidt, J. Brett, S.-D. Yan, F. Wang, Y.-C. Pan, K. Elliston, D. Stern, and A. Shaw. 1992. Cloning and expression of RAGE: a cell surface receptor for advanced glycosylation end products of proteins. *J. Biol. Chem.* 267:14998–15004.
14. Kleinman, H., M. McGarvey, J. Hassell, V. Star, F. Cannon, G. Laurie, and G. Martin. 1986. Basement membrane complexes with biological activity. *Biochemistry*. 25:312–318.
15. Passaniti, A., R. Taylor, R. Pili, Y. Guo, P. Long, J. Haney, R. Pauly, D. Grant, and G. Martin. 1992. A simple quantitative method for assessing angiogenesis and anti-angiogenic agents using reconstituted basement membrane, heparin, and fibroblast growth factor. *Lab. Invest.* 67:519–527.
16. Kenyon, B., E. Voest, C. Chen, E. Flynn, J. Folkman, and R. D'Amato. 1996. A model of angiogenesis in the mouse cornea. *Invest. Ophthalmol. Vis. Sci.* 37:1625–1632.
17. Bolton, A., and W. Hunter. 1973. The labelling of proteins to high specific radioactivities by conjugation to a ^{125}I-containing acylating agent. *Biochem. J.* 133:529–539.
18. Yamoaka, K., T. Nakagawa, and T. Uno. 1978. Application of Akaike's information criterion (AIC) in the evaluation of linear pharmacokinetic equations. *J. Pharmacokinet. Biopharm.* 6:165–175.
19. Weast, R. 1966. Handbook of Chemistry and Physics. The Chemical Rubber Company, Cleveland, OH. 2,000 pp.
20. O'Reilly, M., L. Holmgren, Y. Shing, C. Chen, R. Rosenthal, M. Moses, W. Lane, Y. Cao, E. Sage, and J. Folkman. 1994. Angiostatin: a novel angiogenesis inhibitor that mediates the suppression of metastases by a Lewis lung carcinoma. *Cell*. 79:315–328.
21. Holmgren, L., M. O'Reilly, and J. Folkman. 1995. Dormancy of micrometastases: balanced proliferation and apoptosis in the presence of angiogenesis suppression. *Nat. Med*. 1:149–153.
22. Fidler, I., and L. Ellis. 1994. The implications of angiogenesis for the biology and therapy of cancer metastasis. *Cell*. 79:185–188.
23. Folkman, J. 1989. What is the evidence that tumors are angiogenesis dependent? *J. Natl. Cancer Inst*. 82:4–6.
24. Folkman, J. 1995. Angiogenesis in cancer, vascular, rheumatoid and other diseases. *Nat. Med*. 1:27–31.
25. Murray, C. 1995. Tumour dormancy: not so sleepy after all. *Nat. Med*. 1:117–118.
26. Olive, P., and R. Durand. 1992. Detection of hypoxic cells in a murine tumor with the use of the comet assay. *J. Natl. Cancer Inst*. 84:707–711.
27. Kalra, R., J. Bremner, P. Wood, J. Sansom, C. Counsell, I. Stratford, and G. Adams. 1994. ^{31}P MRS to monitor the induction of tumor hypoxia by the modification of the oxygen affinity of hemoglobin using BW589C. *Int. J. Radiat. Oncol. Biol. Phys*. 29:285–288.
28. Plate, K., G. Breier, H. Weich, and W. Risau. 1992. Vascular endothelial growth factor is a potential tumor angiogenesis factor in human gliomas in vivo. *Nature*. 359:845–848.
29. Warren, R., H. Yuan, M. Matili, N. Gillett, and N. Ferrara. 1995. Regulation by VEGF of human colon cancer tumorigenesis in a mouse model of experimental liver metastasis. *J. Clin. Invest*. 95:1789–1797.
30. Kim, J., B. Li, J. Winer, M. Armanini, N. Gillett, H. Phillips, and N. Ferrara. 1993. Inhibition of VEGF-induced angiogenesis suppresses tumor growth in vivo. *Nature*. 362:841–844.
31. Maciag, T., T. Mehlman, R. Friesel, and A. Schrieber. 1984. Heparin binds endothelial cell growth factor, the principal endothelial cell mitogen in bovine brain. *Science*. 225:932–935.
32. Shing, Y., J. Folkman, R. Sullivan, C. Butterfield, J. Murray, and M. Klagsbrun. 1984. Heparin affinity: purification of a tumor-derived capillary endothelial cell growth factor. *Science*. 223:1296–1298.
33. Fett, J., D. Strydom, R. Lobb, E. Alderman, J. Bethune, J. Riordan, and B. Vallee. 1985. Isolation and characterization of angiogenin, an angiogenic protein from human carcinoma cells. *Biochemistry*. 24:5480–5486.
34. King, T.V., and B. Vallee. 1991. Neovascularisation of the meniscus with angiogenin. An experimental study in rabbits. *J. Bone Joint Surg. [Br.]*. 73B:587–590.
35. Olson, K., T. French, B. Vallee, and J. Fett. 1994. A monoclonal antibody to human angiogenin suppresses tumor growth in athymic mice. *Cancer Res*. 54:4576–4579.
36. Kandel, J., E. Bossy-Wetzel, F. Ravanyi, M. Klagsbrun, J. Folkman, and D. Hanahan. 1991. Neovascularization is associated with a switch to the export of bFGF in the multistep development of fibrosarcoma. *Cell*. 66:1095–1104.
37. Hori, A., R. Sasada, E. Matsutani, K. Naito, Y. Sakura, T. Fujita, and Y. Kozai. 1991. Suppression of solid tumor growth by immunoneutralizing monoclonal antibody against bFGF. *Cancer Res*. 51:6189–6194.
38. Dameron, K., O. Volpert, M. Tainsky, and N. Bouck. 1994. Control of angiogenesis in fibroblasts by p53 regulation of thrombospondin-1. *Science*. 265:1582–1585.
39. Van Meir, E., P. Polverini, V. Chazin, H.-J. Su Huang, N. de Tribolet, and W. Cavenee. 1994. Release of an inhibitor of angiogenesis upon induction of wild-type p53 expression in glioblastoma cells. *Nat. Genet*. 8:171–176.
40. O'Reilly, M., L. Holmgren, C. Chen, and J. Folkman. 1996. Angiostatin induces and sustains dormancy of human primary tumors in mice. *Nat. Med*. 2:689–692.
41. Shweiki, D., A. Itin, D. Soffer, and E. Keshet. 1992. VEGF induced by hypoxia may mediate hypoxia-initiated angiogenesis. *Nature*. 359:843–845.
42. Knighton, D., T. Hunt, H. Scheuenstuhl, B. Halliday, Z. Werb, and M. Banda. 1983. Oxygen tension regulates the expression of angiogenesis factor by macrophages. *Science*. 221:1283–1285.
43. Kuwabara, K., S. Ogawa, M. Matsumoto, S. Koga, M. Clauss, D. Pinsky, L.Witte, J. Joseph-Silverstein, M. Furie, G. Torcia, et al. 1995. Hypoxia-mediated induction of a/bFGF and PDGF in mononuclear phagocytes stimulates growth of hypoxic endothelial cells. *Proc. Natl. Acad. Sci. USA*. 92: 4606–4610.
44. Brogi, E., J. Winkles, R. Underwood, S. Clinton, G. Alberts, and P. Libby. 1993. Distinct patterns of expression of FGFs and their receptors in human atheroma and nonatherosclerotic arteries. *J. Clin. Invest*. 92:2408–2418.
45. Nawroth, P., D. Handley, G. Matsueda, R. DeWaal, H. Gerlach, D. Blohm, and D. Stern. 1988. Tumor necrosis factor/cachectin–induced intravascular fibrin formation in meth A fibrosarcomas. *J. Exp. Med*. 168:637–647.
46. Watanabe, N., Y. Niitsu, H. Umeno, H. Muriyama, H. Neda, N. Yamauchi, M. Maeda, and I. Urushizaki. 1988. Toxic effect of TNF on tumor vasculature in mice. *Cancer Res*. 48:2179–2183.
47. Freudenberg, N., K. Joh, O. Westphal, C. Mittermyer, M. Freudenberg, and C. Galanos. 1984. Haemorrhagic tumour necrosis following endotoxin administration. *Virchows Arch*. 403:377–389.

48. North, R., and E. Havell. 1988. The antitumor function of tumor necrosis factor (TNF) II. Analysis of the role of endogenous TNF in endotoxin-induced hemorrhagic necrosis and regression of an established sarcoma. *J. Exp. Med*. 167:1086–1099.
49. Leibovich, S., P. Polverini, H. Shepard, D. Wiseman, V. Shively, and N. Nuseir. 1987. Macrophage-induced angiogenesis is mediated by TNF-α. *Nature*. 329:630–632.
50. Fraker-Schroder, M., W. Risau, R. Hallmann, P. Gautschi, and P. Bohlen. 1987. TNF-α, a potent inhibitor of endothelial cell growth in vitro, is angiogenic in vivo. *Proc. Natl. Acad. Sci. USA*. 84:5277–5281.
51. Madri, J., L. Bell, and J. Merwin. 1992. Modulation of vascular cell behavior by TGFβ. *Mol. Reprod. Dev*. 32:121–126.